Temporal Evolution of Temperature and Argon Impurity Density Profiles Observed by X-ray Imaging Spectrometer Measurements at Wendelstein 7-X

A. Langenberg[1], N.A. Pablant[2], O. Marchuk[3], P. Valson[1], P. Traverso[4], R. Burhenn[1], A. Alonso[5], D. Zhang[1], B. Buttenschön[1], J. Svensson[1], D. Gates[2], M. Beurskens[1], R.C. Wolf [1], and the W7-X Team

[1] *Max-Planck-Institut für Plasmaphysik,17491 Greifswald, Germany*
[2] *Princeton Plasma Physics Laboratory, Princeton, NJ, USA*
[3] *Institut für Energie und Klimaforschung, Forschungszentrum Jülich GmbH, 52425 Jülich, Germany*
[4] *Auburn University, Auburn, AL, USA*
[5] *Laboratorio Nacional de Fusión – CIEMAT, 28040 Madrid, Spain*

Introduction

In the first operational phase of the stellarator Wendelstein 7-X (W7-X), two x-ray imaging spectrometer systems, the X-ray Imaging Crystal Spectrometer (XICS) [1,2] and the High Resolution X-ray Imaging Spectrometer (HR-XIS) [3,4], have been commissioned. Both systems are designed to provide radial profiles of ion and electron temperature, T_i and T_e, plasma rotation velocities v_P, and selected impurity densities n_Z. This paper shows first measurements of both spectrometers and presents first results of Ar impurity transport studies: Using the Minerva Bayesian analysis framework [5], the evolution of Ar impurity density profiles after an Ar gas puff could be observed with a time resolution of up to 5 ms.

1. Imaging Spectrometers HR-XIS and XICS at W7-X

The XICS and HR-XIS spectrometers have been set up at W7-X in collaborations with the Princeton Plasma Physics Laboratory (XICS) [2] and the Forschungszentrum Jülich (HR-XIS) [4]. Both systems are equipped with spherical bent crystals, imaging x-rays emitted from the plasma onto a two dimensional detector with energy resolution in horizontal, and spatial resolution in vertical direction.

Fig.1 a) shows the designed viewing geometries of XICS and HR-XIS and the spatial range covering radial positions $\rho^{XICS} = 0.84\backslash 0.42$ and $\rho^{\text{HR-XIS}} = 0.25\backslash 0.65$ above\below the magnetic axis. Throughout this paper, ρ denotes the square root of normalized magnetic flux. Depending on the crystal choice and set Bragg angle, spectra of selected impurities, *e.g.* Ar, of a particular charge state can be monitored. Typical raw images for the emission of Ar^{17+} ($L_{\alpha 1/2}$ emission lines) and Ar^{16+} (*w*, *x, y,* and *z* lines) are shown in Fig.1 b), measured for Bragg angles of 49.4° and 54.0°.

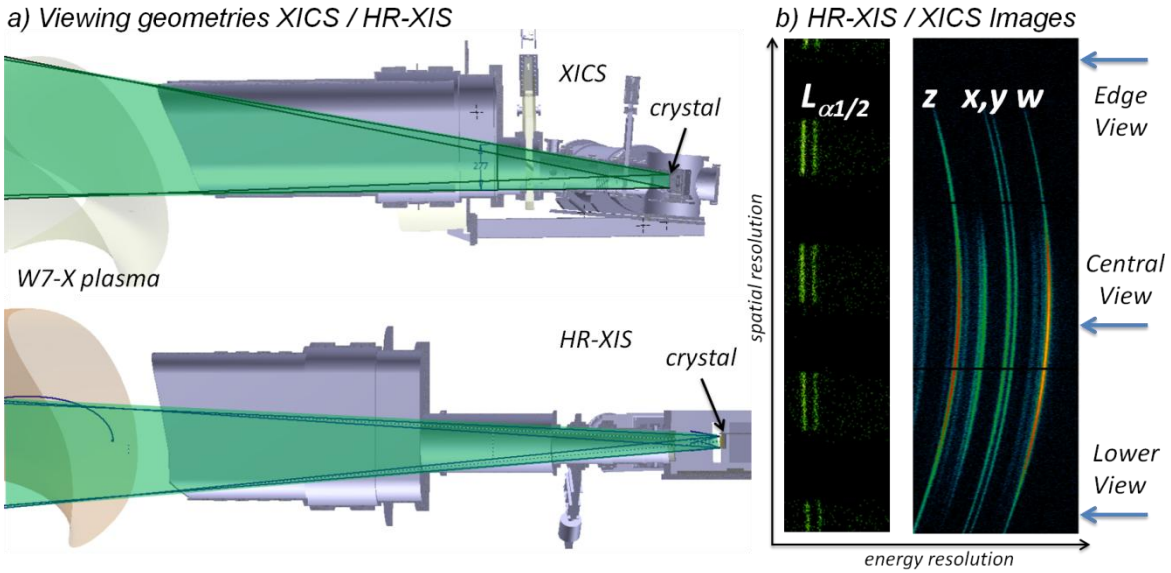

Fig.1: a) Viewing geometries (shaded area) of the XICS and HR-XIS spectrometers at W7-X. b) Recorded images of Ar^{17+} and Ar^{16+} emission on the HR-XIS and XICS detectors.

2. Direct Observation of Highly Charged Argon Density Profiles

A spectral fit of line of sight integrated spectra and a tomographic inversion of XICS data yields profiles of above mentioned plasma parameters as shown in Fig.2. Spectral fits (Fig.2(a), green lines) of measured data (Fig.2(a), blue lines) show an excellent match with

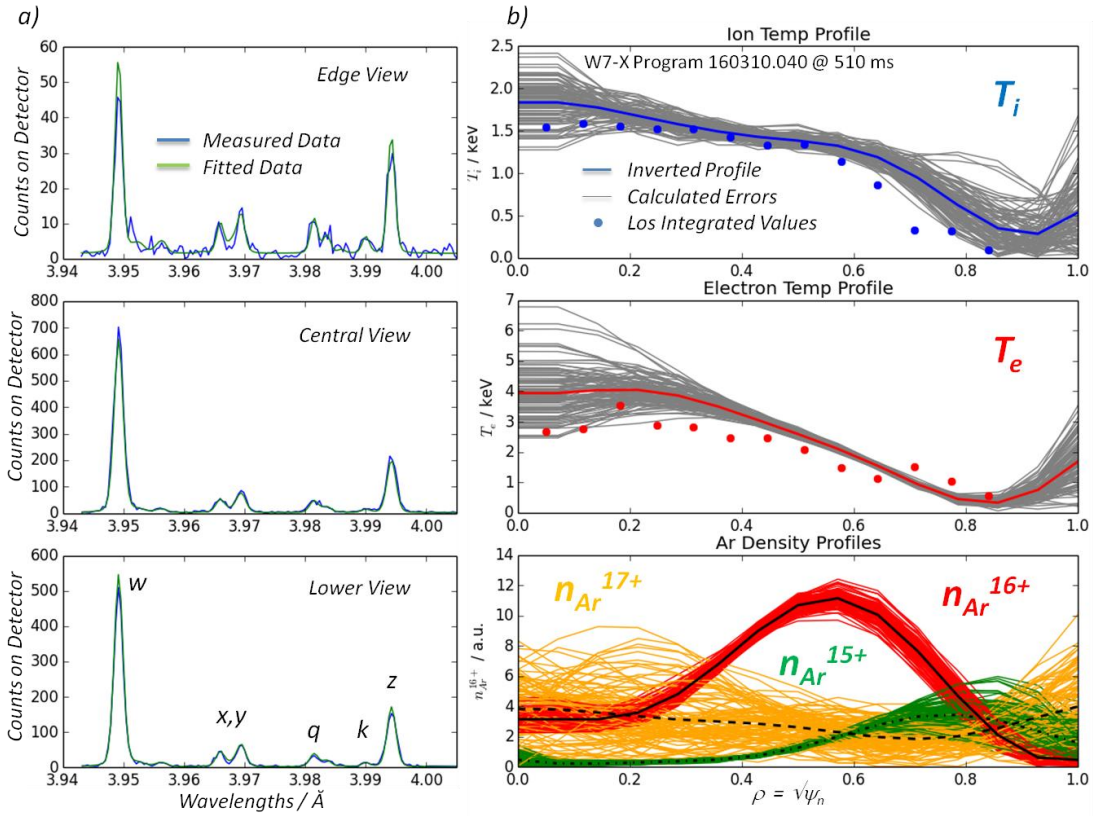

Fig.2: a) Measured and fitted XICS Ar^{16+} spectra along the outermost (edge and lower view) and along the central line of sight. b) Inferred ion and electron temperature (solid lines) and Ar density profiles of different charge states (solid, dashed, and dash-dotted lines) including calculated errors (thin solid lines). Line of sight integrated temperature values are shown as dots.

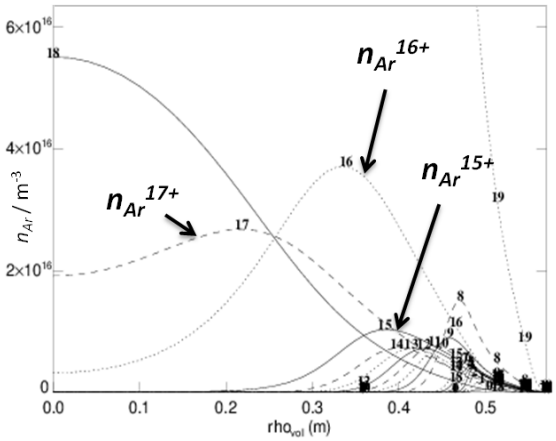

Fig.3: Calculated Ar density profiles using STRAHL transport code, with assumed transport coefficients (see text).

deviations on the order of the photon statistics. From Doppler broadening and line intensity rations of the emission lines, line of sight integrated T_i and T_e values (blue and red dots in Fig.2 b) can be determined directly from the spectral fit. The inference of actual temperature and density profiles has been done with an entire forward model of XICS using Bayesian Analysis for error estimation [1,5]. Thin gray and colored solid lines in Fig.2 b) represent sampled profiles from the error distribution which yield forward modeled XICS data matching measured data within the photon statistics. The simultaneous fit of all emission lines in the spectra, including satellites from recombination and excitation of n_{Ar}^{15+} and n_{Ar}^{17+}, allows to infer n_{Ar}^{15+}, n_{Ar}^{16+}, and n_{Ar}^{17+} profiles (Fig.2b). Effects of charge exchange with the neutral H background gas have been neglected. All Ar densities are given in arbitrary units as an absolute density calibration is not available. However, the relative scaling of different charge states is accurate. According to the fractional abundances of charge states at different T_e, the maxima of n_{Ar}^{15+} to n_{Ar}^{17+} profiles shift from the low T_e edge region towards the high T_e plasma center. Moreover, the penetration depth into the plasma center of n_{Ar}^{16+} is significantly larger compared to n_{Ar}^{15+}. For a first estimate of expected n_{Ar} profiles, a 1D STRAHL [6] transport code calculation has been carried out, using measured n_e and T_e profiles, typical diffusion coefficients (D=0.5 m^2/s), and zero ion drift velocity. The overall profile shapes (Fig.3), including the peaking positions of n_{Ar}^{15+} and n_{Ar}^{16+} profiles, can be resembled within the calculations very well.

3. Ar Gas Puff Experiments

For a more detailed analysis of impurity transport, Ar gas puff experiments have been performed. Therefore, a short Ar gas puff (30 ms) has been put into the plasma at a stationary phase with static T_e and n_e profiles, typically 150 ms after the start of the ECRH heating.

The temporal evolution of n_{Ar}^{15+} and n_{Ar}^{16+} profiles is shown in Fig.4 a) in a 3D plot along the time axis. Starting at 185 ms, a pronounced and fast rise of the Ar density profiles can be observed with a rise time of 30±5 ms.

In the left of Fig.4 b), the uncertainties at selected times (colored thin lines) of inferred n_{Ar}^{15+}, n_{Ar}^{16+}, and n_{Ar}^{17+} profiles (dashed lines) are shown for t = 185-215 ms. For n_{Ar}^{16+}, the errors are smaller or equal to the observed changes in profiles between time steps of 5 ms, for n_{Ar}^{15+} profiles, uncertainties are larger than observed changes in profiles, especially for $\rho > 0.6$.

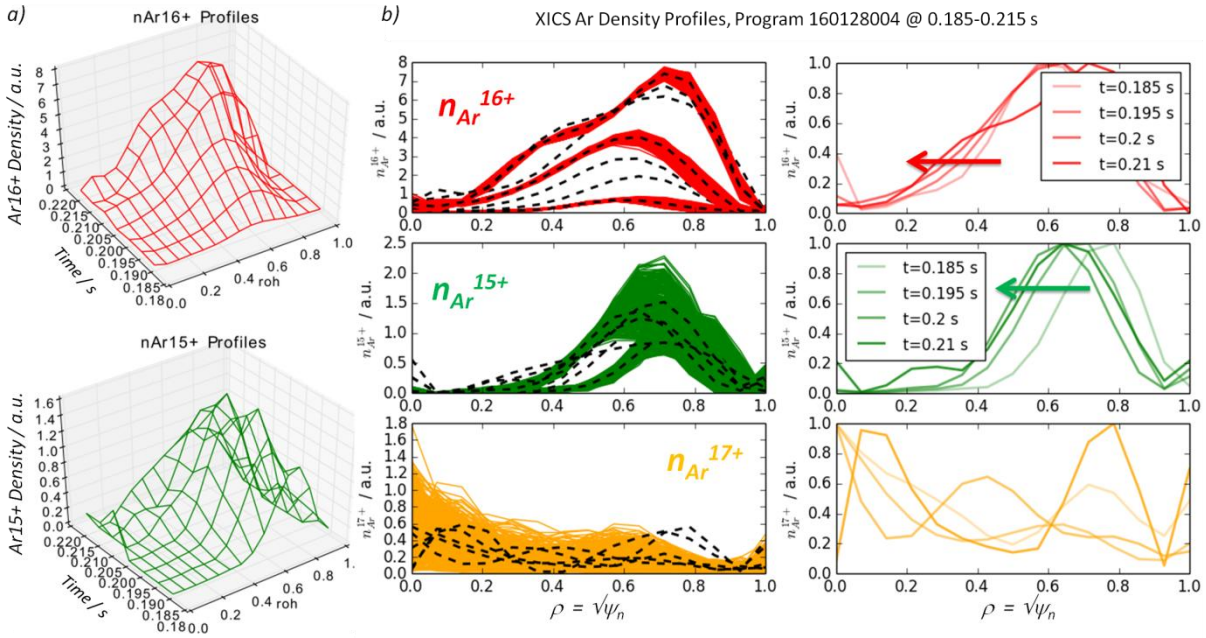

Fig.4: a) Temporal evolution of n_{Ar}^{15+} and n_{Ar}^{16+} profiles after an Ar gas puff. b) Argon density profiles (dashed lines) with calculated uncertainties (colored lines) for selected times (left) and normalized Ar density profiles showing impurity propagation for n_{Ar}^{15+} and n_{Ar}^{16+}(right).

For n_{Ar}^{17+} profiles, a clear temporal evolution cannot be resolved due to high uncertainties originating from the low intensity of satellite lines used for the profile inference.

In order to trace changes in the shapes of density profiles, they have been normalized to their peak values (Fig.4 (b), right). The n_{Ar}^{15+} and n_{Ar}^{16+} profiles show an impurity propagation towards the plasma center after the Ar gas puff as indicated by the arrows, getting stationary for $t > 215$ ms (not shown). For n_{Ar}^{17+}, the statistics are too low to observe a trend. More accurate measurements of n_{Ar}^{17+} could be available using measured H-like spectra of Ar.

Since the actual Ar density distribution inside the plasma depends strongly on impurity transport processes, a detailed analysis of the Ar density profiles in the three observed charge states and the temporal evolution of its shapes should give deeper insight into neoclassical transport and possible anomalous transport effects by comparison with transport calculations.

Acknowledgments

This work has been carried out within the framework of the EUROfusion Consortium and has received funding from the Euratom research and training programme 2014-2018 under grant agreement No 633053. The views and opinions expressed herein do not necessarily reflect those of the European Commission.

[1] A. Langenberg, J. Svensson, H. Thomsen et al., Fusion Sci. Technol. **69**, 560 (2016)

[2] N.A. Pablant, M. Bitter, R. Burhenn et al. in 41st EPS Conf. on Plasma Phys., **38F** (2014) p. 1.076

[3] A. Langenberg, H. Thomsen et al., in 41st EPS Conf. on Plasma Phys., **38F** (2014) p. 1.074

[4] G. Bertschinger, W. Biel, H. Jaegers et al. Review of Scientific Instruments **75,** 3727 (2004)

[5] J. Svensson, A. Werner, IEEE International Symposium on Intelligent Signal Processing, (2007)

[6] R. Dux, IPP report 10/30 (2006); K. Behringer, JET report JET-R 87 08 (1987)